ACS APPLIED ENERGY MATERIALS

www.acsaem.org

Letter

Direct Air Capture-Compatible Azolate and Amino Acid Ionic Liquids for Electrochemical CO_2 Reduction to CO on a Silver Cathode

Priyadarshini Seshasayee, Nishu Devi, Chang Liu, Lauren Crochet, Anna Bunger, Juliane Weber,* and Sankar Nair*

Cite This: *ACS Appl. Energy Mater.* 2026, 9, 5880−5887

Read Online

ACCESS | Metrics & More | Article Recommendations | Supporting Information

ABSTRACT: Direct air capture (DAC) compatible ionic liquids (ILs) are attractive for integrating CO_2 capture and conversion due to their high CO_2 solubility at low partial pressures, tunable chemisorption mechanisms, low volatility, and wide electrochemical windows. However, very few ILs have high CO_2 uptake at DAC conditions (420 ppm CO_2), and even fewer have been evaluated for chemical compatibility and mechanistic continuity for combined capture and electrochemical CO_2 reduction (eCO_2RR). We demonstrate that two representative DAC-capable ILs, $[P_{4444}][Val]$ (amino acid-based) and $[P_{66614}][5\text{-Me-Imd}]$ (azolate-based), exhibit favorable electrochemical reduction behavior. CO and H_2 were the dominant gas-phase products by GC, while ^1H and ^{13}C NMR confirmed negligible liquid-phase HCOOH. Chronoamperometry at moderate applied potentials (−2.0 to −2.5 V vs Ag/AgCl) in a two-compartment H-cell with a Ag coated carbon paper as the working electrode yielded steady-state current densities of ∼10 mA cm^{-2} with CO FE of 96% for $[P_{4444}][Val]$ and 95% for $[P_{66614}][5\text{-Me-Imd}]$, highlighting the role of viscosity and chemically absorbed CO_2-IL species to provide highly selective CO formation while suppressing H_2 evolution.

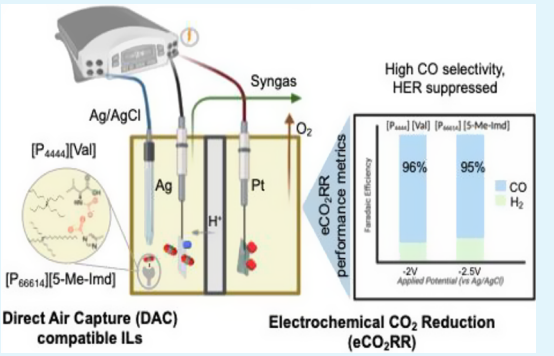

KEYWORDS: *direct air capture, electrochemical CO_2 reduction, azolate ionic liquid, amino acid ionic liquid, silver electrocatalyst*

■ INTRODUCTION

Carbon dioxide (CO_2) emissions are a leading contributor to the greenhouse effect and climate change, threatening environmental stability and economic resilience.[1] Current mitigation strategies include (1) reducing emissions via low-carbon fuels and renewable energy; (2) developing CO_2 capture and storage systems; and (3) utilizing CO_2 as a feedstock to produce valuable chemicals and fuels.[2] Conventional sorbent-based capture methods (thermal, pressure, or moisture-swing cycles) are energy-intensive,[3] e.g., in direct air capture (DAC) of CO_2 from ambient air (∼420 ppm; ≈4.2 × 10^{-4} bar pCO_2), thermal swing unit consumes ∼95% of energy input and ∼75% of process capital, with purified CO_2 >$200/ton, whereas integrated capture–conversion has the potential to reduce costs to $20–25/ton.[3] The electrochemical CO_2 reduction reaction (eCO_2RR) directly converts captured CO_2 into CO, HCOOH, CH_4, CH_3OH, and C_2 hydrocarbons using renewable electricity,[3−5] and when coupled with DAC, it enables near net-zero emissions.[6−8] Achieving this, however, requires electrolytes that capture CO_2 efficiently at ambient levels and enable highly selective eCO_2RR. At such low partial pressures, limited CO_2 solubility restricts delivery to the electrode, favoring the hydrogen evolution reaction (HER). Traditional aqueous (bi)carbonate systems are further constrained by low CO_2 solubility (∼33 mM at 1 atm), mass-transport limits, and local pH shifts,[6,9,10] reducing current densities and selectivity under DAC conditions.[11] Recent work demonstrated the first DAC-to-eCO_2RR coupling in alkaline KOH, converting air-captured CO_2 in a BPM cell to formate (16% FE) using SnO_2/C and CO (13% FE) using the Ag/C electrocatalyst at 50 mA cm^{-2}.[12] However, performance is restricted by low dissolved inorganic carbon (DIC) loading, alkalinity loss from (bi)carbonate precipitation, and high voltages inherent to BPM operation.[13] These constraints motivate non-aqueous, DAC-compatible media that couple capture with selective eCO_2RR conversion.

Ionic liquids (ILs) have emerged as attractive non-aqueous electrolytes for eCO_2RR due to their high CO_2 solubility at low partial pressures, tunable chemisorption, low volatility, and wide electrochemical windows.[3,14] Structurally, ILs are salts composed of bulky organic cations such as imidazolium,

Received: January 11, 2026
Revised: April 11, 2026
Accepted: April 17, 2026
Published: April 27, 2026

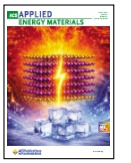

https://doi.org/10.1021/acsaem.6c00117
ACS Appl. Energy Mater. 2026, 9, 5880−5887

ammonium, or phosphonium, paired with diverse anions including halides, amino acids (AA-ILs), and functionalized heterocycles (such as azolate-based aprotic heterocyclic anions, AHA-ILs). ILs interact with CO_2 through physical and chemical absorption, allowing more precise tuning for integrated capture and conversion.[12,15–17] Functional groups capable of reversible CO_2 interactions, combined with the ionic conductivity of ILs, can facilitate CO_2 activation by lowering its energy barrier.[2,3] Thus, ILs enhance CO_2RR selectivity while suppressing the HER.[3,14]

Prior studies have largely evaluated ILs under high CO_2 concentrations (5–15%) relevant to flue gas capture[12,18–20] where solubility and kinetics are less limiting, while DAC conditions (~420 ppm CO_2) remain scarcely explored. Although simulations predict promising DAC performance for AHA-ILs such as [P_{66614}][5-Me-Imd],[21] these estimates rely on empirical correction factors for uptakes than direct measurements and remain experimentally unvalidated. Experimental DAC demonstrations with amino acid ILs (e.g., [N_{4444}][BCAA], [N_{4444}][Arg]) have focused exclusively on thermal capture–regeneration cycles,[22,23] with no prior studies examining DAC-relevant IL chemistry performance under eCO_2RR. Early eCO_2RR studies focused on azolate-based ILs with non-coordinating anions (such as [BF_4], [NTf_2], and [PF_6]), typically dissolved in acetonitrile or H_2O with additives such as K_2CO_3 or supplementary ILs, where the ILs interacted through weak, physisorptive interactions with CO_2, requiring higher potentials (−1.9 to −2.5 V vs Ag/Ag^+) and higher IL loadings (0.7 to 0.9 M IL in H_2O/acetonitrile) to achieve moderate CO FE (40–80%), limited by CO_2 solubility and the HER.[24–28] In contrast, ILs with reactive anions combine chemisorption and physisorption, lowering overpotentials while improving current densities and FE, with product selectivity governed by the electrocatalyst. For example, [P_{66614}][124-Triaz] allows 95% HCOOH FE at −0.7 V on Ag, while [BMIM][124-Triaz] and [P_{4444}][4-MF-PhO] give >93% FE for HCOOH (6% FE oxalate) at −2.0 V on Pb.[3,14] Although these ILs have low DAC CO_2 uptakes (i.e., they are not DAC-compatible), such results highlights the role of CO_2-reactive anions in enabling lower-energy reduction pathways.[14] The only IL demonstrated for combined low-concentration capture (at ~5000 ppm CO_2) and eCO_2RR conversion so far is [EMIM][2-CNPyr].[19,20,29]

Here, we report the first experimental demonstration of two DAC-compatible ionic liquids, tetrabutylphosphonium valinate [P_{4444}][Val] and trihexyltetradecylphosphonium 5-methylimidazolate [P_{66614}][5-Me-Imd], that strongly chemisorb CO_2 at ambient pressures and subsequently support selective electrochemical CO_2-to-CO conversion following modest formulation adjustments. Notably, this work presents the first demonstration of amino-acid-based ionic liquids achieving both DAC-level CO_2 capture and electrochemical conversion. It establishes the dual compatibility of these ionic liquids through two sequential unit operations: CO_2 capture under DAC-relevant conditions using neat ionic liquids and IL-supporting electrolyte formulations relevant to the electrochemical environment, followed by eCO_2RR after targeted addition of a solvent to enhance ionic conductivity and mass transport. Importantly, the compatibility of the eCO_2RR electrolyte formulation for reuse in the capture step is also evaluated. This framework establishes mechanistic continuity between capture and conversion and positions these ionic liquids as promising candidates for fully integrated DAC-to-electrolytic conversion processes.

EXPERIMENTAL SECTION

The Supporting Information (pp. S2–S5) provides a complete description of all experimental methods and procedures.

RESULTS AND DISCUSSION

The ILs [P_{4444}][Val] and [P_{66614}][5-Me-Imd] (structures shown in Figure 1) were synthesized via equimolar ion exchange (Supporting Information). The CO_2 uptake under dilute conditions was evaluated with a custom temperature-swing bubbler (Figure 1a). In this setup, 12% CO_2 (balance N_2) and pure N_2 were mixed at a specific flow rate ratio to obtain a stream with 420 ppm CO_2 (303 K), which was bubbled through the neat IL, maintained in a thermostated oil bath. The CO_2-depleted exit stream was analyzed by an LI-COR 850 CO_2/H_2O infrared analyzer, with uptake capacity determined by integrating the blank vs IL breakthrough curves. At 303 K and 420 ppm CO_2 (Figure 1b), [P_{4444}][Val] demonstrated an uptake of 0.44 mol CO_2/mol IL (1.16 mol/kg), while [P_{66614}][5-Me-Imd] showed 0.14 mol CO_2/mol IL (0.24 mol/kg). The two ILs represent chemically distinct families: [P_{4444}][Val] is an amino acid IL (AA-IL) and captures CO_2 via reversible interactions, while [P_{66614}][5-Me-Imd] is an azolate IL that undergoes nucleophilic CO_2 attack at the nitrogen atom of the anion. Although AA-ILs exhibit high CO_2 uptake, they are rarely studied electrochemically due to high viscosity after CO_2 binding.

Pre-exposure viscosities for [P_{4444}][Val] and [P_{66614}][5-Me-Imd] are comparable (236 cP and 243 cP at 303 K, respectively), but diverge significantly after CO_2 uptake, with [P_{4444}][Val] exhibiting a pronounced increase. [P_{4444}][Val] forms gel-like phases through hydrogen bonding, impairing CO_2 mass transport, conductivity, wettability, and CO_2 diffusion.[30] Therefore, the 1:1 (CO_2:IL) stoichiometry promotes dense amine–carbamate networks that would limit dynamic electrochemical operation. In contrast, [P_{66614}][5-Me-Imd] maintains stable viscosity during CO_2 uptake due to its hydrophobic, aprotic nature.[31] To confirm the CO_2–IL interactions, 100% CO_2 was bubbled through 1:2 v/v IL:DMSO-d_6 solutions for 16 hours, and standard NMR spectra were acquired with 64 scans (4 s relaxation delay). The ^{13}C NMR spectra before/after CO_2 exposure (Figure 1c–f) confirm carbamate formation. [P_{4444}][Val] shows a new valinate–carbamate peak at 157.49 ppm from its primary amine, while [P_{66614}][5-Me-Imd] shows a imidazolate–carbamate peak at 166 ppm. Corresponding ^{13}C NMR spectrum peaks are shown in the SI.

The CO_2 uptake of [P_{4444}][Val] at 50% CO_2 (0.5 bar) and 303 K was 0.78 mol CO_2/mol IL (2.07 mol/kg), while [P_{66614}][5-Me-Imd] showed 0.67 mol CO_2/mol IL (1.19 mol/kg), both of the same order of magnitude as their DAC-level uptakes, indicating a strong CO_2 binding affinity under dilute conditions. Having shown the high uptakes of these two ILs at DAC-relevant concentrations, we conducted eCO_2RR under pure CO_2 conditions to determine overall electrochemical behavior including both chemical and physical absorption. In prior eCO_2RR studies of [P_{66614}][124-Triaz] with the Ag/Ag^+ reference, current densities were <1 mA cm^{-2} up to ~−2 V vs Ag/Ag^+, due to IL viscosity, limiting ionic mobility, and conductivity.[14] This underscores the need for IL molecular tuning to reduce viscosities or co-solvent addition. Adding water to a DES ([Ch][Cl]: ethylene glycol) reduced viscosity by three orders of magnitude,[12] thus boosting current

https://doi.org/10.1021/acsaem.6c00117
ACS Appl. Energy Mater. 2026, 9, 5880−5887

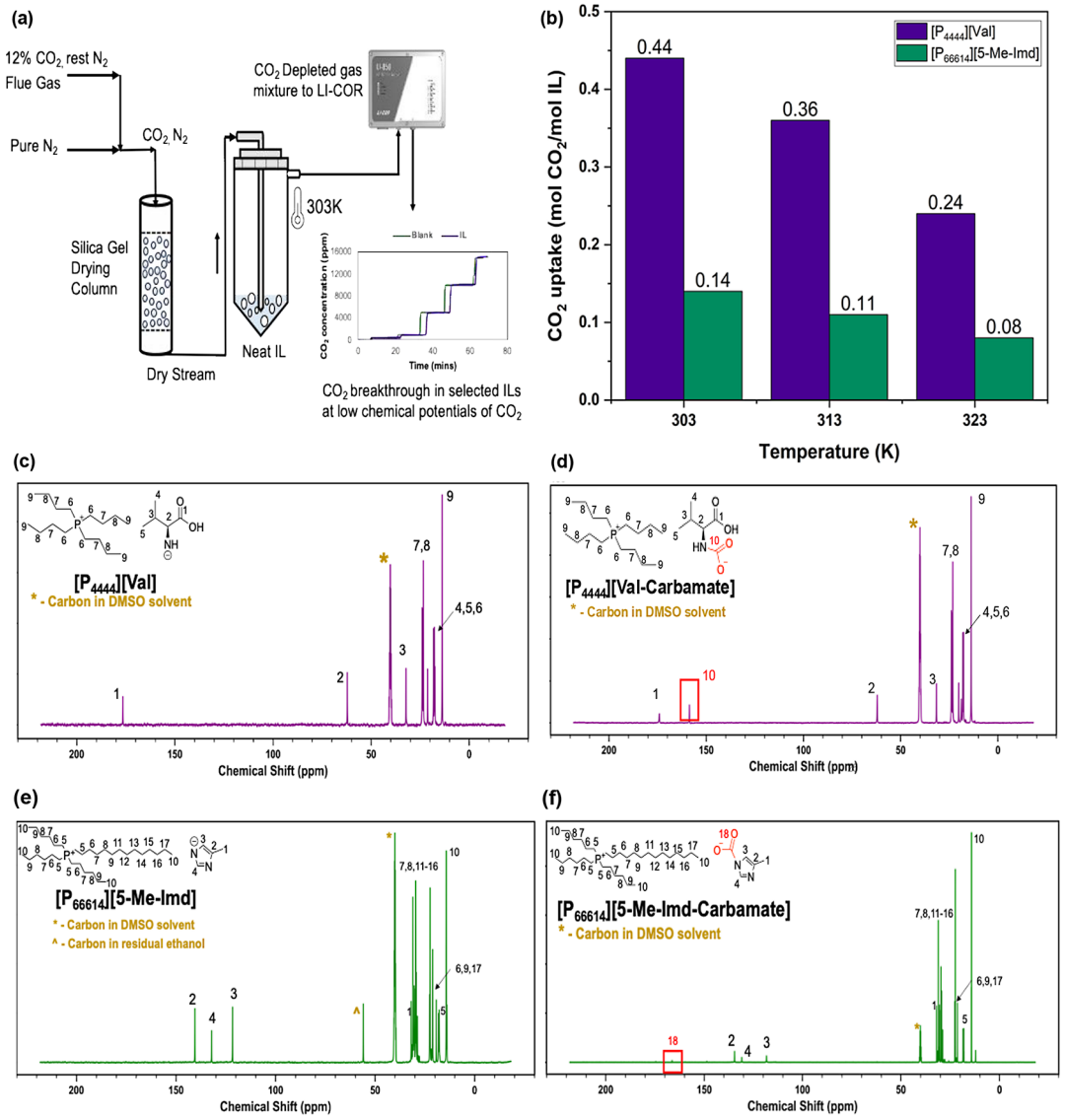

Figure 1. (a) Temperature-swing bubbler setup for low-pCO_2 absorption breakthrough in ILs for uptake measurement. (b) Experimental CO_2 uptake (mol CO_2/mol IL) of $[P_{4444}][Valine]$ and $[P_{66614}][5\text{-Me-Imd}]$ with 420 ppm CO_2 in N_2 at 303, 313, and 323 K. (c) ^{13}C NMR of neat $[P_{4444}][Val]$ with annotated carbons and structure. (d) ^{13}C NMR spectra of $[P_{4444}][Val]$ after CO_2 exposure showing a new carbamate peak. (e) ^{13}C NMR spectra of neat $[P_{66614}][5\text{-Me-Imd}]$ with structure, showing trace amounts of residual ethanol left from the synthesis step. (f) ^{13}C NMR spectra of CO_2-exposed $[P_{66614}][5\text{-Me-Imd}]$ with a new carbamate peak.

but also promoting the HER and lowering CO selectivity (~23% at –1.6 V). Aprotic solvents instead improved both electrochemical activity and CO selectivity.[3] Motivated by this, we used acetonitrile (ACN) for its low viscosity (~0.34–0.37 cP at 25 °C), high CO_2 diffusivity (~2–4 × 10^{-5} cm^2 s^{-1}), and a wide electrochemical window, enhancing ionic mobility and stability under reductive conditions while minimizing background currents.[29] At low IL loadings (0.1–0.3 M), IL–ACN mixtures exhibit viscosities of ~0.4–0.7 cP, supporting favorable mass transport.[2] To further reduce resistance (Ohmic drop), tetraethylammonium perchlorate (TEAP) was added as a supporting electrolyte, establishing a well-defined medium to evaluate intrinsic IL activity and selectivity.[3,32] Typically eCO_2RR performance for CO_2-to-CO over Ag working electrodes in H-cell configurations,[31] particularly at low IL loadings and moderate catalyst loadings, yielded moderate current densities below 10 mA cm^{-2}. In contrast, reports of >95% CO Faradaic efficiency at current densities exceeding 100 mA cm^{-2} generally rely on engineered electrocatalysts (e.g., single-atom catalysts[13]), optimized electrolyzer architectures,[33] or tailored ionic liquid formulations that reduce viscosity, enhance ionic conductivity, and increase local CO_2 availability.[3,34] The electrochemical setup (Figure S1a) employed a two-compartment H-cell separated by a Nafion NR-212 cation-exchange membrane (CEM). Details of the setup and electrode preparation are described in the SI.[27,35]

To establish a baseline, we first examined the control catholyte (0.1 M TEAP in acetonitrile, ACN) under CO_2-saturated conditions. Devoid of chemisorptive moieties, this system isolates CO_2 physisorption and background reduction.[29] As shown in Figure S1b, geometric current density increased from –1.85 mA/cm^2 at –1.5 V to –69 mA/cm^2 at –3.5 V

https://doi.org/10.1021/acsaem.6c00117
ACS Appl. Energy Mater. 2026, 9, 5880–5887

(vs Ag/AgCl). CA curves (Figure S1c) confirmed steadily increasing currents with applied potential, reflecting enhanced electrocatalytic activity. The physisorbed CO_2 produced CO and H_2 with no liquid-phase products detected via NMR (Figure S4), consistent with reduction of dissolved CO_2. In the control electrolyte, the summed FE (Figure S1d) occasionally exceeded 100% (e.g. at −1.5 V) or fell below 100% at more negative potentials. Such deviations are common in eCO_2RR and can arise from capacitive currents, side reactions, or crossover effects.[36] We emphasize that the relative product trends in FE and gas selectivity (Figure S1d,e) remain robust across replicates, although absolute FE values deviate.[31] CO FE dominates over H_2 at moderate overpotentials (−2 to −2.5 V vs Ag/AgCl) as seen from Figure S1d,e, consistent with physisorbed CO_2 being preferentially reduced on Ag. Beyond −2.5 V, however, the HER becomes increasingly competitive, lowering CO FE and shifting selectivity toward H_2. Physically absorbed CO_2 is reduced to CO on the Ag/C WE via the classical two-electron pathway (Table S1, SI). In aprotic ACN, protons originate from the 0.5 M H_2SO_4 anolyte and migrate through the CEM, sustaining reduction and charge balance. On the Ag WE, CO_2 adsorbs, forms a CO_2 radical, and protonates to CO. Silver stabilizes the CO_2^- intermediate while suppressing the HER, yielding high CO selectivity under moderate overpotentials. FE and gas selectivity performance at −2.0 to −2.5 V (vs Ag/AgCl) likely reflects a favorable balance of moderate overpotential, CO_2 availability, and suppressed HER. At more negative potentials, electric double layer compression increases proton access and side reactions, consistent with prior TEAP/ACN studies.[29] Beyond −2.5 V, the HER dominates despite greater driving force, consistent with prior reports that TEAP/ACN stability is strongly potential-dependent[29,32] Although CO selectivity appears high at −2.0 and −2.5 V, the corresponding CO FE is only 20–35%, due to the limited efficiency of physisorbed CO_2 reduction in the control electrolyte (Figure S1d). Under DAC conditions, where physical solubility is far lower, this performance would deteriorate further, highlighting the need for ILs that chemically bind CO_2 to sustain activity.[30]

Next, measurements were performed with 0.1 M $[P_{4444}][Val]$ in 0.1 M TEAP/ACN, which lowered viscosity relative to neat ILs but remained higher than that of the control. Figure 2a,b shows that reduction currents were suppressed compared to the control across all potentials, plateauing near −9 mA/cm^2 at −2 V (about half of the control), consistent with reduced CO_2 diffusivity and mass-transport limitations associated with the viscosity of AA-IL.[19] Notably, under DAC-relevant conditions,

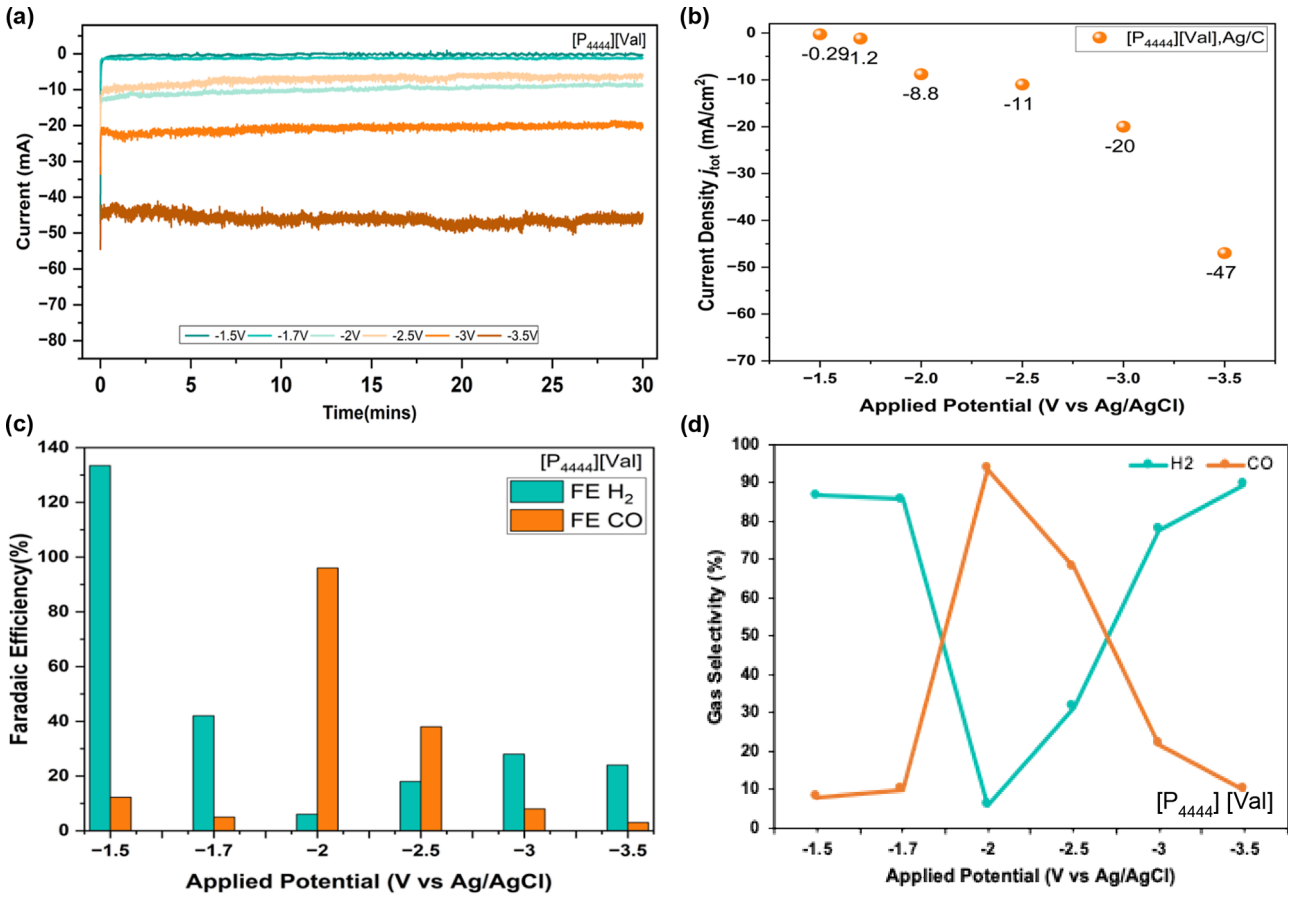

Figure 2. eCO_2RR with $[P_{4444}][Val]$ (0.1 M) + TEAP (0.1 M) in acetonitrile. Conditions: identical to control, 1 cm^2 Ag/C WE, CO_2 flow 100 sccm (pre-bubbling) and then 20 sccm. (a) CA curves show suppressed currents due to higher viscosity; (b) current densities remain lower at all potentials; (c) FE of H_2 and CO, with CO FE peaks at 96% at −2.0 V and then declines. (d) Gas selectivity of H_2 and CO; CO selectivity reaches 97.0% at −2.0 V, indicating enhanced specificity despite reduced current efficiency. *Note*: Data reported for this case is from a single independent measurement. See Figure 3 for error bars, which are expected to be similar in both IL cases. Summed FE occasionally deviates from 100% due to common H-cell artifacts (gas dissolution, GC quantification limits, and capacitive currents); NMR analysis confirms no ionic liquid degradation or additional liquid products (Figures S5–S7).

https://doi.org/10.1021/acsaem.6c00117
ACS Appl. Energy Mater. 2026, 9, 5880−5887

$[P_{4444}][Val]$ can sustain CO_2 availability through chemical binding, in contrast to the purely physisorptive control electrolyte. Gas analysis confirms CO and H_2 as the dominant products, as supported by ^1H NMR analysis of the catholyte at −2.0 V (Figures S5 and S6), with only trace HCOOH detected. At −2.0 V vs Ag/AgCl, CO FE reached 96% (Figure 2c), and the CO selectivity was ∼97% compared to ∼80% in control (Figure 2d). Despite reduced current densities compared to control, $[P_{4444}][Val]$ directs the reduction pathway to CO formation. This selectivity enhancement arises from chemisorption of CO_2 at the valinate anion to form valine–carbamate species (Table S2), which enrich CO_2 equivalents near the electrode interface while reducing effective proton availability and suppressing the HER at moderate overpotentials.[14,32] At more negative potentials, both FE and selectivity for CO declined, as in other Ag/CO_2RR systems where the HER becomes dominant.[29,37] Trace HCOOH at −3.5 V may account for part of the FE gap but remained negligible overall.

While $[P_{4444}][Val]$ demonstrates proof of concept that chemisorptive ILs can favor CO formation even under transport-limited conditions, a key practical drawback of AA-ILs is their tendency to form insoluble valine−carbamate precipitates upon prolonged CO_2 exposure[18,38−41] (Figure S7). These amorphous solid carbamates dissolve poorly in ACN, creating heterogeneous electrolytes that reduce ion mobility, disrupt electrode contact, deplete CO_2 equivalents from solution, and alter effective electrolyte composition. Such precipitation-induced electrolyte evolution likely contributes to the declining CO FE and selectivity observed at high overpotentials, highlighting a key limitation of AA-IL systems for sustained electrochemical operation. To address these limitations, we next investigated $[P_{66614}][5\text{-Me-Imd}]$, an aprotic heterocyclic anion IL (AHA-IL), that captures CO_2 via nucleophilic attack at the azolate nitrogen, forming azolate−carbamate species without the extensive hydrogen-bonding networks characteristic of AA-ILs.[12,19,21,42] Unlike AA-ILs, AHA-ILs maintain low, stable viscosity during CO_2 uptake.[43] At the dilute concentrations employed here (0.1 M in ACN), viscosity remains nearly constant (∼0.4–0.7 cP), enabling DAC-relevant chemisorption while maintaining favorable transport properties.[2]

The electrochemical behavior of $[P_{66614}][5\text{-Me-Imd}]$ (Figure 3) exhibited suppressed, flattened currents across

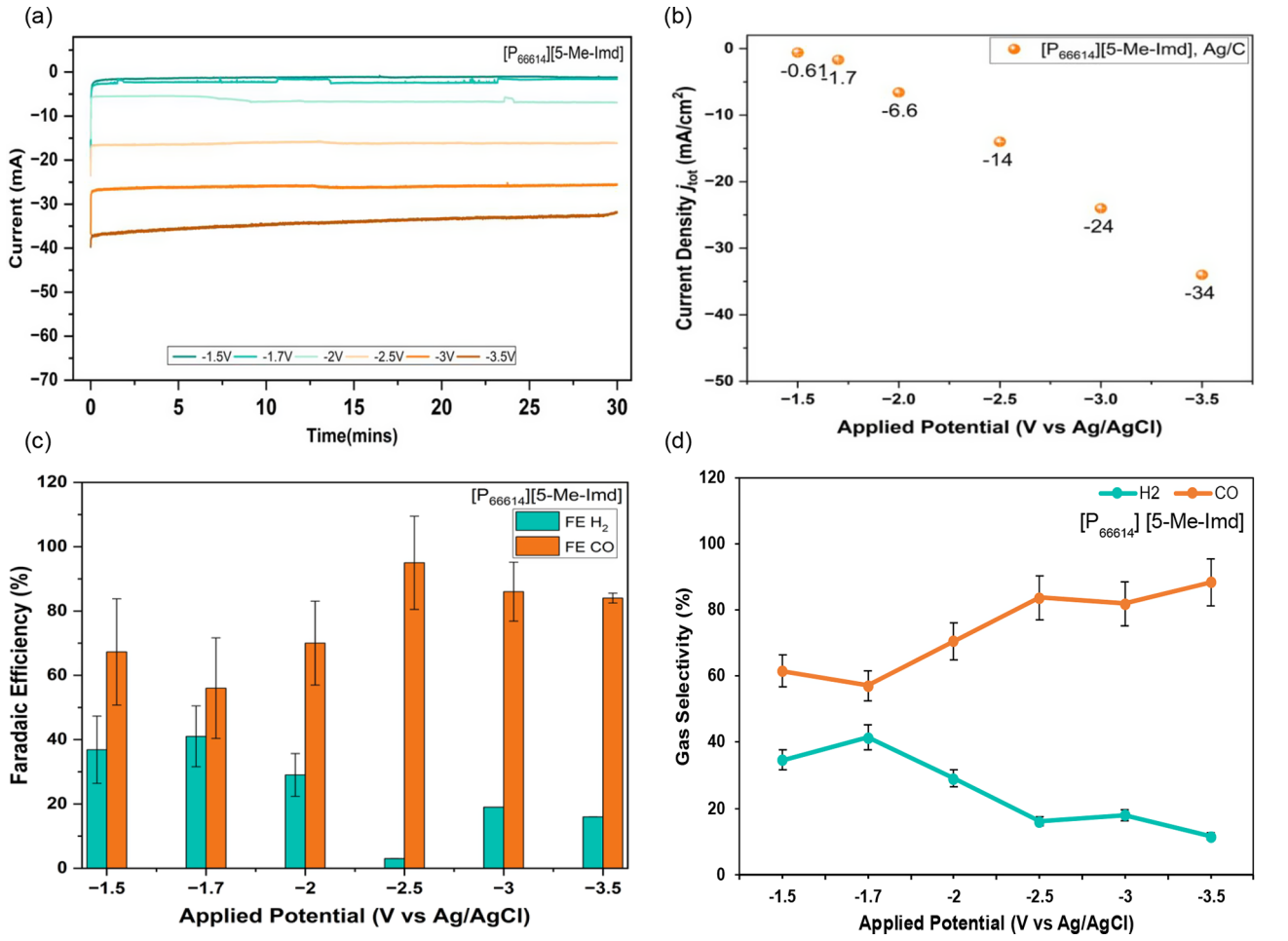

Figure 3. eCO_2R R with $[P_{66614}][5\text{-Me-Imd}]$ (0.1 M) + TEAP (0.1 M) in acetonitrile. Conditions identical to the control (1 cm^2 Ag/C WE, CO_2 flow at 100 sccm during pre-bubbling and then 20 sccm). (a) CA curves show suppressed currents from higher viscosity; (b) current densities remain lower across all potentials and error bars are represented in white markers within the range ± 10%; (c) FE of H_2 and CO, with CO FE exceeding 95% at −2.5 V before declining; and (d) selectivity trends showing CO selectivity reaching 84% at −2.0 V, indicating enhanced specificity despite reduced current efficiency. Error bars represent the standard deviation from three independent electrolysis experiments; variability in H_2 FE and selectivity was negligible at higher overpotentials.

https://doi.org/10.1021/acsaem.6c00117
ACS Appl. Energy Mater. 2026, 9, 5880−5887

−1.5 to −3.5 V vs Ag/AgCl compared to the control, reflecting mass transport limitations in IL-containing electrolytes, similar to AA-ILs (Figure 3a,b). At −2.0 V, the control reaches −17 mA cm^{-2}, while the $[P_{4444}][Val]$ and $[P_{66614}][5\text{-Me-Imd}]$ yielded lower and comparable currents of −8.8 and −6.6 mA cm^{-2}, respectively, consistent with their similar initial viscosities under dilute conditions. However, as CO_2 binding progresses, the two systems diverge markedly. Although $[P_{4444}][Val]$ undergoes pronounced electrolyte evolution due to precipitation of poorly soluble valine–carbamate species and an increasing electrolyte viscosity, $[P_{66614}][5\text{-Me-Imd}]$ maintains a homogeneous catholyte with stable viscosity. CO_2 is retained in solution as a combination of physisorbed CO_2 and soluble imidazole–carbamate species, preserving a homogeneous reservoir of CO_2 equivalents throughout electrolysis, enabling sustained electrochemical operation. Product analysis confirms CO and H_2 as the dominant gaseous products. ^1H NMR spectra (Figures S8 and S9) show the negligible liquid-phase reduction product, including HCOOH. As shown in Figure 3c,d, $[P_{66614}][5\text{-Me-Imd}]$ strongly favors CO formation over a broad potential window. At −2.5 V vs Ag/AgCl, CO Faradaic efficiency exceeds 95% with ∼88% CO selectivity, while H_2 remains below ∼10%. FE error bars represent the standard deviation obtained from three independent repeats (see Table S3). This behavior reflects the ability of azolate anions to chemically bind CO_2, increasing its local concentration and stabilizing CO_2 intermediates, while simultaneously disfavoring proton reduction. Notably, at more negative potentials (−3.0 and −3.5 V vs Ag/AgCl), CO Faradaic efficiency and selectivity remain comparatively high (∼80%) despite increased driving force for the HER, even as the total current density rises (Figure 3b). This behavior contrasts with AA-ILs and is attributed to the formation of soluble imidazole–carbamate species that maintain CO_2 availability in the electrolyte and prevent precipitation-induced depletion of CO_2 equivalents. As a result, CO_2RR remains the dominant reaction pathway even under high cathodic bias, enabling simultaneous achievement of high CO selectivity and elevated current densities.

In a fully integrated process, the DAC capture step would be performed using the equimolar IL + TEAP mixture, without acetonitrile (ACN). Post-DAC, ACN would be added to reduce viscosity and improve mass transport for eCO_2RR. In an integrated system, ACN would be recovered from the liquid outlet stream by separations such as organic solvent nanofiltration and/or stripping, whereas vapor-phase ACN would be recovered by condensation. These separation processes would be heat-integrated (e.g., using heat pumps or exchangers) for energy savings. Furthermore, to assess compatibility between capture and electrochemical operation, CO_2 breakthrough curves were measured for neat IL ($[P_{66614}][5\text{-Me-Imd}]$) and the equimolar IL + TEAP formulation used during CO_2RR (Figure S10). Introduction of TEAP slows the initial uptake kinetics, consistent with dilution of reactive sites and increased ionic strength; however, the IL + TEAP formulation ultimately achieves a higher total capacity than the neat IL. This sorption behavior reflects the presence of chemical CO_2 binding by the azolate anion and enhanced physical CO_2 dissolution enabled by increased free volume in the IL+ TEAP environment. In phosphonium-based systems containing highly aliphatic cations such as $[P_{66614}]^+$ or $[P_{4444}]^+$, disruption of local ion packing by the TEA^+ cation further promotes physical solubility through the formation of additional microdomains by increasing free-volume elements capable of accommodating dissolved CO_2.[15,44] Importantly, ^{13}C NMR spectra collected after CO_2 exposure for the IL+TEAP system (Figure S11) show no new resonances beyond those of imidazole–carbamate species, confirming that TEAP remains chemically inert and contributes exclusively through physical dissolution. Collectively, these results demonstrate that the IL + TEAP formulation is DAC-compatible and in fact enables enhanced capture capacity while preserving chemical integrity for subsequent eCO_2RR.

Additional electrochemical and structural characterization further supports the mechanistic distinctions between the two IL systems (Schemes S1 and S2). Long-term electrolysis stability tests and scan-rate dependent LSVs of the catholyte are provided in Figure S12. Morphological analysis of the Ag/C electrode before and after electrolysis (Figures S13–S17) shows clear differences between the two electrolytes. In the $[P_{4444}][Val]$ system, localized surface agglomerates consistent with valine–carbamate deposition are observed after electrolysis, whereas the $[P_{66614}][5\text{-Me-Imd}]$ system maintains a cleaner catalyst surface with well-dispersed Ag nanoparticles. These observations are consistent with the precipitation behavior of amino acid ILs and the homogeneous speciation of azolate-based ILs during CO_2 reduction.

■ CONCLUSIONS

In summary, this study experimentally confirms the mechanistic continuity and chemical compatibility of DAC-relevant CO_2 capture in functional ionic liquids ($[P_{4444}][Val]$ and $[P_{66614}][5\text{-Me-Imd}]$) with subsequent electrochemical CO_2 reduction. While $[P_{4444}][Val]$ offers high CO_2 uptake (∼0.44 mol CO_2/mol IL at 420 ppm) and promotes CO formation (95% CO FE and 8.8 mA cm^{-2} at −2.0 V vs Ag/AgCl) at moderate overpotentials, precipitation of insoluble valine–carbamate species increases viscosity, depletes electroactive CO_2, and limits long-term electrochemical stability. In contrast, $[P_{66614}][5\text{-Me-Imd}]$ maintains stable viscosity and maintains a soluble imidazolium–carbamate speciation, preserving a homogeneous electrolyte that supports sustained CO-selective reduction (>95% FE, ∼88–90% selectivity at −2.5 V vs Ag/AgCl and >80% FE above −3 V vs Ag/AgCl) across a broad potential window. Moreover, the absence of precipitation ensures cleaner operation, improved stability, and consistent interfacial behavior. eCO_2RR performance at 420 ppm CO_2 is expected to remain robust, since the control already indicates a ∼20% CO FE contribution from physisorbed CO_2 at moderate overpotentials, providing an upper bound for FE variation under DAC conditions. Together, these findings identify azolate-based ILs as robust and scalable alternatives to amino acid ILs for CO_2 electroreduction, particularly in applications where selectivity, long-term operational stability, and catholyte compatibility are critical.

■ ASSOCIATED CONTENT

Supporting Information

The Supporting Information is available free of charge at https://pubs.acs.org/doi/10.1021/acsaem.6c00117.

Experimental methods; ionic liquid synthesis and characterization; the CO_2 absorption setup and breakthrough analysis; NMR spectra (^1H and ^{13}C) before and after CO_2 exposure; the electrochemical setup and procedures;

https://doi.org/10.1021/acsaem.6c00117
ACS Appl. Energy Mater. 2026, 9, 5880−5887

additional CA, LSV, and Faradaic efficiency data; long-term stability measurements; scan-rate-dependent voltammetry; control electrolyte analysis; supplementary tables; SEM images of Ag/C electrodes before and after CO_2RR; particle size distribution; and additional schematics and mechanistic illustrations (PDF)

AUTHOR INFORMATION

Corresponding Authors

Juliane Weber – *Chemical Sciences Division, Oak Ridge National Laboratory, Oak Ridge, Tennessee 37830, United States;* orcid.org/0000-0001-7961-0220; Email: weberj@ornl.gov

Sankar Nair – *School of Chemical and Biomolecular Engineering, Georgia Institute of Technology, Atlanta, Georgia 30332, United States;* orcid.org/0000-0001-5339-470X; Email: sankar.nair@chbe.gatech.edu

Authors

Priyadarshini Seshasayee – *School of Chemical and Biomolecular Engineering, Georgia Institute of Technology, Atlanta, Georgia 30332, United States;* orcid.org/0009-0005-4407-3724

Nishu Devi – *Chemical Sciences Division, Oak Ridge National Laboratory, Oak Ridge, Tennessee 37830, United States*

Chang Liu – *Chemical Sciences Division, Oak Ridge National Laboratory, Oak Ridge, Tennessee 37830, United States*

Lauren Crochet – *School of Chemical and Biomolecular Engineering, Georgia Institute of Technology, Atlanta, Georgia 30332, United States*

Anna Bunger – *School of Chemical and Biomolecular Engineering, Georgia Institute of Technology, Atlanta, Georgia 30332, United States*

Complete contact information is available at: https://pubs.acs.org/doi/10.1021/acsaem.6c00117

Notes

The authors declare no competing financial interest.

ACKNOWLEDGMENTS

This work was supported as part of Understanding and Controlling Accelerated and Gradual Evolution of Materials for Energy (UNCAGE-ME), an Energy Frontier Research Center funded by the U.S. Department of Energy, Office of Science, Basic Energy Sciences under Award # DE-SC0012577. Scanning electron microscopy characterization was conducted as part of a user project at the Center for Nanophase Materials Sciences (CNMS), which is a US Department of Energy, Office of Science User Facility at Oak Ridge National Laboratory.

REFERENCES

(1) Center for Climate and Energy Solutions *Global Emissions*. https://www.c2es.org/content/international-emissions.

(2) Fortunati, A.; Risplendi, F.; Re Fiorentin, M.; Cicero, G.; Parisi, E.; Castellino, M.; Simone, E.; Iliev, B.; Schubert, T. J. S.; Russo, N.; Hernández, S. Understanding the Role of Imidazolium-Based Ionic Liquids in the Electrochemical CO_2 Reduction Reaction. *Commun. Chem.* **2023**, *6*, 84.

(3) Dongare, S.; Zeeshan, M.; Aydogdu, A. S.; Dikki, R.; Kurtoglu-Oztulum, S. F.; Coskun, O. K.; Munoz, M.; Banerjee, A.; Gautam, M.; Ross, R. D.; Stanley, J. S.; Brower, R. S.; Muchharla, B.; Sacci, R. L.; Velazquez, J. M.; Kumar, B.; Yang, J. Y.; Hahn, C.; Keskin, S.; Morales-Guio, C. G.; Uzun, A.; Spurgeon, J. M.; Gurkan, B. Reactive Capture and Electrochemical Conversion of CO_2 with Ionic Liquids and Deep Eutectic Solvents. *Chem. Soc. Rev.* **2024**, *53* (17), 8563–8631.

(4) Tan, X.; Sun, X.; Han, B. Ionic Liquid-Based Electrolytes for CO_2 Electroreduction and CO_2 Electroorganic Transformation. *Natl. Sci. Rev.* **2022**, *9* (4), No. nwab022.

(5) Jia, S.; Ma, X.; Sun, X.; Han, B. Electrochemical Transformation of CO_2 to Value-Added Chemicals and Fuels. *CCS Chem.* **2022**, *4* (10), 3213–3229.

(6) Venkataraman, A.; Song, H.; Brandão, V. D.; Ma, C.; Casajus, M. S.; Fernandez Otero, C. A.; Sievers, C.; Hatzell, M. C.; Bhargava, S. S.; Arora, S. S.; Villa, C.; Dhingra, S.; Nair, S. Process and Techno-Economic Analyses of Ethylene Production by Electrochemical Reduction of Aqueous Alkaline Carbonates. *Nat. Chem. Eng.* **2024**, *1* (11), 710–723.

(7) Chen, C.; Khosrowabadi Kotyk, J. F.; Sheehan, S. W. Progress toward Commercial Application of Electrochemical Carbon Dioxide Reduction. *Chem.* **2018**, *4* (11), 2571–2586.

(8) Yang, Z.; Li, X.; Cui, X.; Zheng, Z.; Zheng, P.; Zhang, Y. Integrated Strategies Toward the Capture and Electrochemical Conversion of Low-Concentration Carbon Dioxide. *Exploration* **2025**, *5*, No. e20240006.

(9) Marcandalli, G.; Monteiro, M. C. O.; Goyal, A.; Koper, M. T. M. Electrolyte Effects on CO_2 Electrochemical Reduction to CO. *Acc. Chem. Res.* **2022**, *55* (14), 1900–1910.

(10) Monteiro, M. C. O.; Philips, M. F.; Schouten, K. J. P.; Koper, M. T. M. Efficiency and Selectivity of CO_2 Reduction to CO on Gold Gas Diffusion Electrodes in Acidic Media. *Nat. Commun.* **2021**, *12*, 4943.

(11) Zhu, Z.; Tang, W.; Wang, J.; Zhao, L.; Lin, Y.; Li, Z.; Niu, X.; Chen, J. S.; Wu, R. Insights into Operating Conditions on Electrocatalytic CO_2 Reduction. *Adv. Energy Mater.* **2025**, *15* (16), No. 2405768.

(12) Vasilyev, D. V.; Rudnev, A. V.; Broekmann, P.; Dyson, P. J. A General and Facile Approach for the Electrochemical Reduction of Carbon Dioxide Inspired by Deep Eutectic Solvents. *ChemSusChem* **2019**, *12* (8), 1635–1639.

(13) Wu, Y.; Chen, C.; Yan, X.; Sun, X.; Zhu, Q.; Li, P.; Li, Y.; Liu, S.; Ma, J.; Huang, Y.; Han, B. Boosting CO_2 Electroreduction over a Cadmium Single-Atom Catalyst by Tuning of the Axial Coordination Structure. *Angew. Chem., Int. Ed.* **2021**, *60* (38), 20803–20810.

(14) Hollingsworth, N.; Taylor, S. F. R.; Galante, M. T.; Jacquemin, J.; Longo, C.; Holt, K. B.; De Leeuw, N. H.; Hardacre, C. Reduction of Carbon Dioxide to Formate at Low Overpotential Using a Superbase Ionic Liquid. *Angew. Chem., Int. Ed.* **2015**, *54* (47), 14164–14168.

(15) Zeng, S.; Zhang, X.; Bai, L.; Zhang, X.; Wang, H.; Wang, J.; Bao, D.; Li, M.; Liu, X.; Zhang, S. Ionic-Liquid-Based CO_2 Capture Systems: Structure, Interaction and Process. *Chem. Rev.* **2017**, *117* (14), 9625–9673.

(16) Bates, E. D.; Mayton, R. D.; Ntai, I.; Davis, J. H. CO_2 Capture by a Task-Specific Ionic Liquid. *J. Am. Chem. Soc.* **2002**, *124* (6), 926–927.

(17) Shukla, S. K.; Khokarale, S. G.; Bui, T. Q.; Mikkola, J.-P. T. Ionic Liquids: Potential Materials for Carbon Dioxide Capture and Utilization. *Front. Mater.* **2019**, *1*, 42.

(18) Ramdin, M.; De Loos, T. W.; Vlugt, T. J. H. State-of-the-Art of CO_2 Capture with Ionic Liquids. *Ind. Eng. Chem. Res.* **2012**, *51*, 8149–8177.

(19) Gurkan, B.; Goodrich, B. F.; Mindrup, E. M.; Ficke, L. E.; Massel, M.; Seo, S.; Senftle, T. P.; Wu, H.; Glaser, M. F.; Shah, J. K.; Maginn, E. J.; Brennecke, J. F.; Schneider, W. F. Molecular Design of High Capacity, Low Viscosity, Chemically Tunable Ionic Liquids for CO_2 Capture. *J. Phys. Chem. Lett.* **2010**, *1* (24), 3494–3499.

(20) Lee, Y. Y.; Edgehouse, K.; Klemm, A.; Mao, H.; Pentzer, E.; Gurkan, B. Capsules of Reactive Ionic Liquids for Selective Capture

of Carbon Dioxide at Low Concentrations. *ACS Appl. Mater. Interfaces* **2020**, *12* (16), 19184–19193.
(21) Hospital-Benito, D.; Moya, C.; Gazzani, M.; Palomar, J. Direct Air Capture Based on Ionic Liquids: From Molecular Design to Process Assessment. *Chem. Eng. J.* **2023**, *468*, No. 143630.
(22) Recker, E. A.; Green, M.; Soltani, M.; Paull, D. H.; Mcmanus, G. J.; Davis, J. H.; Mirjafari, A. Direct Air Capture of CO_2 via Ionic Liquids Derived from "Waste" Amino Acids. *ACS Sustainable Chem. Eng.* **2022**, *10* (36), 11885–11890.
(23) Bera, N.; Sardar, P.; Samanta, A. N.; Sarkar, N. Arginine-Based Ionic Liquid in a Water-DMSO Binary Mixture for Highly Efficient CO_2 Capture from Open Air. *Energy Fuels* **2024**, *38* (2), 1281–1287.
(24) Rosen, B. A.; Salehi-Khojin, A.; Thorson, M. R.; Zhu, W.; Whipple, D. T.; Kenis, P. J. A.; Masel, R. I. Ionic Liquid-Mediated Selective Conversion of CO_2 to CO at Low Overpotentials. *Science* **2011**, *334* (6056), 643–644.
(25) Asadi, M.; Kumar, B.; Behranginia, A.; Rosen, B. A.; Baskin, A.; Repnin, N.; Pisasale, D.; Phillips, P.; Zhu, W.; Haasch, R.; Klie, R. F.; Král, P.; Abiade, J.; Salehi-Khojin, A. Robust Carbon Dioxide Reduction on Molybdenum Disulphide Edges. *Nat. Commun.* **2014**, *5*, 4470.
(26) Liu, B.; Guo, W.; Gebbie, M. A. Tuning Ionic Screening to Accelerate Electrochemical CO_2 Reduction in Ionic Liquid Electrolytes. *ACS Catal.* **2022**, *12* (15), 9706–9716.
(27) Henckel, D. A.; Saha, P.; Rajana, S.; Baez-Cotto, C.; Taylor, A. K.; Liu, Z.; Resch, M. G.; Masel, R. I.; Neyerlin, K. C. Understanding Limitations in Electrochemical Conversion to CO at Low CO_2 Concentrations. *ACS Energy Lett.* **2024**, *9* (7), 3433–3439.
(28) Sun, L.; Ramesha, G. K.; Kamat, P. V.; Brennecke, J. F. Switching the Reaction Course of Electrochemical CO_2 Reduction with Ionic Liquids. *Langmuir* **2014**, *30* (21), 6302–6308.
(29) Dongare, S.; Coskun, O. K.; Cagli, E.; Stanley, J. S.; Mir, A. Q.; Brower, R. S.; Velázquez, J. M.; Yang, J. Y.; Sacci, R. L.; Gurkan, B. Key Experimental Considerations When Evaluating Functional Ionic Liquids for Combined Capture and Electrochemical Conversion of CO_2. *Langmuir* **2024**, *40* (18), 9426–9438.
(30) Gutowski, K. E.; Maginn, E. J. Amine-Functionalized Task-Specific Ionic Liquids: A Mechanistic Explanation for the Dramatic Increase in Viscosity upon Complexation with CO_2 from Molecular Simulation. *J. Am. Chem. Soc.* **2008**, *130* (44), 14690–14704.
(31) Keller, A. N.; Thacker, P. J.; Baldea, M.; Stadtherr, M. A.; Brennecke, J. F. Reaction Thermochemistry for Carbon Dioxide Absorption by Aprotic N-Heterocyclic Anion Ionic Liquids. *ACS Sustainable Chem. Eng.* **2024**, *12* (36), 13634–13644.
(32) Dongare, S.; Coskun, O. K.; Cagli, E.; Lee, K. Y. C.; Rao, G.; Britt, R. D.; Berben, L. A.; Gurkan, B. A Bifunctional Ionic Liquid for Capture and Electrochemical Conversion of CO_2 to CO over Silver. *ACS Catal.* **2023**, *13* (12), 7812–7821.
(33) Wang, L.; Wu, Y. Advancing Electrocatalytic CO_2 Reduction: Key Strategies for Scaling up to Industrial Applications. *Nanoscale* **2025**, *17* (29), 16988–17003.
(34) Li, Y.; Li, F.; Laaksonen, A.; Wang, C.; Cobden, P.; Boden, P.; Liu, Y.; Zhang, X.; Ji, X. Electrochemical CO_2 Reduction with Ionic Liquids: Review and Evaluation. *Ind. Chem. Mater.* **2023**, *1* (3), 410–430.
(35) Goodrich, B. F.; De La Fuente, J. C.; Gurkan, B. E.; Zadigian, D. J.; Price, E. A.; Huang, Y.; Brennecke, J. F. Experimental Measurements of Amine-Functionalized Anion-Tethered Ionic Liquids with Carbon Dioxide. *Ind. Eng. Chem. Res.* **2011**, *50* (1), 111–118.
(36) Kempler, P. A.; Nielander, A. C. Reliable Reporting of Faradaic Efficiencies for Electrocatalysis Research. *Nat. Commun.* **2023**, *14* (1), 1158.
(37) Re Fiorentin, M.; Risplendi, F.; Salvini, C.; Zeng, J.; Cicero, G.; Jónsson, H. Silver Electrodes Are Highly Selective for CO in CO_2 Electroreduction Due to Interplay between Voltage Dependent Kinetics and Thermodynamics. *J. Phys. Chem. Lett.* **2024**, *15* (46), 11538–11545.
(38) Gurkan, B. E.; De La Fuente, J. C.; Mindrup, E. M.; Ficke, L. E.; Goodrich, B. F.; Price, E. A.; Schneider, W. F.; Brennecke, J. F. Equimolar CO_2 Absorption by Anion-Functionalized Ionic Liquids. *J. Am. Chem. Soc.* **2010**, *132* (7), 2116–2117.
(39) Goodrich, B. F.; De La Fuente, J. C.; Gurkan, B. E.; Lopez, Z. K.; Price, E. A.; Huang, Y.; Brennecke, J. F. Effect of Water and Temperature on Absorption of CO_2 by Amine-Functionalized Anion-Tethered Ionic Liquids. *J. Phys. Chem. B* **2011**, *115*, 9140–9150.
(40) Camper, D.; Bara, J. E.; Gin, D. L.; Noble, R. D. Room-Temperature Ionic Liquid−Amine Solutions: Tunable Solvents for Efficient and Reversible Capture of CO_2. *Ind. Eng. Chem. Res.* **2008**, *47* (21), 8496–8498.
(41) Zhang, X.; Zhang, X.; Dong, H.; Zhao, Z.; Zhang, S.; Huang, Y. Carbon Capture with Ionic Liquids: Overview and Progress. *Energy Environ. Sci.* **2012**, *5* (5), 6668–6681.
(42) Seo, S.; Quiroz-Guzman, M.; DeSilva, M. A.; Lee, T. B.; Huang, Y.; Goodrich, B. F.; Schneider, W. F.; Brennecke, J. F. Chemically Tunable Ionic Liquids with Aprotic Heterocyclic Anion (AHA) for CO_2 Capture. *J. Phys. Chem. B* **2014**, *118* (21), 5740–5751.
(43) Rahim, A.; Yunus, N. M.; Bustam, M. A. Ionic Liquids Hybridization for Carbon Dioxide Capture: A Review. *Molecules* **2023**, *28* (20), 7091.
(44) Liu, X.; O'Harra, K. E.; Bara, J. E.; Turner, C. H. Solubility Behavior of CO_2 in Ionic Liquids Based on Ionic Polarity Index Analyses. *J. Phys. Chem. B* **2021**, *125* (14), 3665–3676.

https://doi.org/10.1021/acsaem.6c00117
ACS Appl. Energy Mater. 2026, 9, 5880−5887